RSC Advances

PAPER

View Article Online
View Journal | View Issue

Cite this: *RSC Adv.*, 2019, **9**, 21018

Preparation of a nanoporous Cu–Ag solid solution with enhanced sono-Fenton-like catalytic activity†

Ning Wang, *[ab] Zhangzhong Wang,[ab] Yajie Chu,[ab] Jialin Cheng,[ab] Hao Yu,[ab] Jindu Huang,[c] Renjie Huo[d] and Chunli Guo[e]

Received 1st May 2019
Accepted 30th June 2019

DOI: 10.1039/c9ra03247a

rsc.li/rsc-advances

Uniform 3D bi-continuous nanoporous Cu–Ag solid solution (NPCS) and nanoporous copper (NPC) were successfully synthesized by dealloying $Cu_{70}Y_{28}Ag_2$ and $Cu_{72}Y_{28}$ metallic glasses, respectively, which was confirmed by using X-ray diffraction (XRD), X-ray photoelectron spectroscopy (XPS), scanning electron microscopy (SEM) and transmission electron microscopy (TEM). The SEM and TEM images show that the ligament size of NPCS (d_{SEM} = 65 nm, d_{TEM} = 45 nm) is much smaller than that of NPC (d_{SEM} = 402 nm, d_{TEM} = 370 nm), which reveals that the ligaments of NPC can be significantly refined by the substitution of 2 at% Ag for Cu in the amorphous precursor. The obtained NPCS exhibits much larger specific surface area and higher total pore volume (S_{BET} = 8.34 m^2 g^{-1}, V_p = 0.093 cm^3 g^{-1}) compared to NPC (S_{BET} = 1.77 m^2 g^{-1}, V_p = 0.050 cm^3 g^{-1}). Furthermore, the catalytic activities of the samples were evaluated by decomposing methyl orange (MO) dye under the irradiation of ultrasound. The results show that NPCS with an extreme fine microstructure displayed superior sono-Fenton-like catalytic activity compared to NPC and commercial copper foil.

1. Introduction

Advanced oxidation process (AOP)[1–3] is one of the most popular approaches used for textile industry wastewater treatment. Among all AOPs, the photocatalytic method is usually adopted due to its convenience.[4,5] However, it is difficult to degrade opaque or translucent dye wastewater by this method because the penetrating ability of the light is limited.[6] In consideration of the strong penetrating ability of ultrasound for any medium,[7] a highly efficient sono-Fenton-like process[8] induced by ultrasonic irradiation was carried out. Ma *et al.*[9] used commercial zero-valent copper to build the sono-Fenton-like system; a significantly enhanced NOR removal was obtained and almost complete removal of NOR was achieved at 30 min. Vaishnave *et al.*[10] reported that the azure-B dye can be efficiently and completely degraded into CO_2 and H_2O through the sono-Fenton-like process.

In the Fenton-like system, transition metal catalyst was need to react with hydrogen peroxide (H_2O_2) to produce high active hydroxyl radicals (·OH).[11] Unfortunately, traditional metal powder catalyst is hard to be recycled, while metal foil has low catalytic activity owing to its small specific surface area.[6] Therefore, nanoporous metals (NPM) with both large specific surface area and high recovery can be an excellent choice for constructing sono-Fenton-like catalytic system. In recent decades, many methods (template, hydrothermal and dealloying) were used to fabricate nanoporous metals.[12–15] Among them, dealloying has been considered to be the most promising method because it is readily available for obtaining various nanoporous metals with 3D bi-continuous structures. For example, Rizzi *et al.*[16] reported that uniform nanoporous gold (NPG) can easily be prepared by dealloying $Au_{40}Cu_{28}Si_{20}Ag_7Pd_5$ glassy alloys, Jin *et al.*[17] reported that monolithic nanoporous silver (NPS) can be fabricated through dealloying of $Ag_{60.5}Ca_{39.5}$ amorphous ribbons, and Wang *et al.*[18] reported that homogeneous nanoporous copper (NPC) can be synthesized *via* chemical dealloying $Cu_{74}Ce_{26}$ metallic glasses.

Compared with nanoporous noble metals (nanoporous gold (NPG),[19] nanoporous silver (NPS),[20] nanoporous palladium (NPPd),[21] nanoporous platinum (NPPt)[22]), nanoporous copper (NPC) and nanoporous Cu-based solid solution material are more attractive owing to both cost-effectiveness and high catalytic activity.[18] More importantly, as an efficient transition metal catalyst, copper as well as iron is often used in Fenton/Fenton-like catalytic process.[10,23,24] In view of the facts that iron can not be existed in the form of nanoporous metals (NPM), which are very applicable for the sono-Fenton-like catalytic process, nanoporous Cu-based material should be a better choice. Among all the nanoporous Cu-based material, nanoporous Cu–Ag solid solution can be the perfect candidate material to construct sono-Fenton-like catalytic system,

[a]School of Materials Science and Engineering, Nanjing Institute of Technology, Nanjing 211167, PR China. E-mail: ymzsts1495@outlook.com; Fax: +86 15951727781; Tel: +86 15951727781

[b]Jiangsu Key Laboratory of Advanced Structural Materials and Application Technology, Nanjing 211167, PR China

[c]School of Materials Science and Engineering, Southeast University, Jiangsu Key Laboratory for Advanced Metallic Materials, Nanjing 211189, PR China

[d]Department of Mechanic Engineering, Guidaojiaotong Polytechnic Institute, Shenyang 110023, PR China

[e]College of Materials Science and Engineering, Taiyuan University of Technology, Taiyuan 030024, PR China

† Electronic supplementary information (ESI) available. See DOI: 10.1039/c9ra03247a

which can be attributed to the following three points: (1) silver is a stable noble metal. Hence, nanoporous Cu–Ag solid solution has better oxidation resistance compared with pure nanoporous copper, thus increasing the stability of nanoporous metal materials. Moreover, silver is much cheaper than other stable noble metals (gold, palladium and platinum). (2) The surface diffusion coefficient of Ag atoms is much lower than that of Cu atoms, which can act as a diffusion barrier to restrict the long distance diffusion of Cu atoms in the dealloying process.[25] Consequently, nanoporous Cu–Ag solid solution fabricated by dealloying possesses very fine microstructure, thus leading to a high sono-catalytic activity.[6] (3) Nanoporous Cu–Ag solid solution of uniform composition and microstructure can be obtained by dealloying: Ag and Cu elements have the same chemical properties, the substitution of Ag element for Cu element in Cu-based metallic glasses can improve its glass forming ability (GFA).[26] The resulting fully amorphous alloys have a unique disordered atomic structure without grain boundaries, dislocations and segregations,[27,28] which is readily available for dealloying synthesis of uniform nanoporous materials.

There are some reports about dealloying synthesis of nanoporous Cu–Ag alloys. Dan *et al.*[25] have synthesized nanoporous Cu–Ag alloys with Ag atoms concentrated at the grain boundary through dealloying of the $Cu_{39}Ti_{60}Ag_1$ and $Cu_{38}Ti_{60}Ag_2$ glassy alloys in hydrofluoric acid (HF) solutions. Unfortunately, highly toxic HF solution was used in this dealloying process, which can pollute the human environment and threaten people's health. Li *et al.*[29] have prepared a 3D nanoporous bimetallic Cu–Ag alloy with some Cu atoms separated from the metastable nanoporous matrix *via* chemical dealloying $Mg_{65}Ag_{12.5}Cu_{12.5}Y_{10}$ amorphous ribbons in sulphuric acid (H_2SO_4) aqueous solution. Which is yet unsatisfying is that the preparation procedure of $Mg_{65}Ag_{12.5}Cu_{12.5}Y_{10}$ alloy ingots is very complex, it involves the smelting of Cu–Y pre-alloy and the melting of volatile Mg, hence the alloy ingots need be produced by using both arc-melting furnace and high-frequency induction furnace. Furthermore, for above two dealloying techniques, the synthesized nanoporous Cu–Ag alloys are uneven, Ag or Cu atoms can be found in the dealloying products. In this work, easily obtained $Cu_{70}Y_{28}Ag_2$ metallic glasses were used as precursors and non-toxic dilute H_2SO_4 solution was used as aggressive medium to prepare uniform nanoporous Cu–Ag solid solution (NPCS), and then the fabricated NPCS was applied in the sono-Fenton-like catalytic degradation of methyl orange (MO). To the best of our knowledge, this is the first report about the sono-Fenton-like process of nanoporous Cu–Ag solid solution.

2. Experimental

The ingots of $Cu_{72-x}Y_{28}Ag_x$ ($x = 0$ and 2 at%, the alloy composition is represented in nominal atomic percentage of the pure elements mixture) were prepared by arc melting a mixture of pure Cu, Y and Ag elements with purities above 99.99 wt% in a Ti-gettered argon atmosphere, followed by a single roller spinning to obtain amorphous ribbons with a width of 2 mm and a thickness of 20–30 μm. Then the ribbons were cut into 3–4 cm in length and immersed in 1 M H_2SO_4 solution for 90 min. The solution was kept at 333 K by a water bath. After dealloying, the corrosion ribbons were rinsed with distilled water and dehydrated alcohol for 10 times and kept in vacuum chamber until characterizations.

The phase composition and chemical valence of the samples were characterized by X-ray diffraction (XRD) using a D8-Discover diffractometer with Cu-K_α radiation ($\lambda = 1.5406$ Å) and X-ray photoelectron spectroscopy (XPS) using a PHI-5000 Versa Probe spectrometer with Al-K_α radiation ($h\gamma = 1486.6$ eV), respectively. The microstructures of obtained dealloying specimens were investigated by FEI-3D scanning electron microscopy (SEM) and G2-20 transmission electron microscopy (TEM), respectively. The size of the metal ligaments was statistically measured by a single length chord method over 100 sites of SEM/TEM morphologies. In addition, a Quantachrome Autosorb-IQ2 analyzer was used to measure the specific surface area (S_{BET}) and total pore volume (V_p) of the nanoporous materials.

The sonocatalytic activities of the samples were evaluated by the degradation of MO under the irradiation of the ultrasound. In this experiment, 100 mL MO solution (20 mg L^{-1}), 50 mg catalyst and 0.5 mL 30 wt% hydrogen peroxide (H_2O_2) were put into a 250 mL Erlenmeyer flask. Prior to the irradiation, the whole suspension was stirred in the dark for 30 min to ensure the establishment of the adsorption–desorption equilibrium. Then, the degradation reactions were conducted in a serial-ultrasonic apparatus (KH-300DB, Kunshan Ultrasonic Apparatus Company, China) with a frequency of 40 kHz and output power of 4800 mW cm^{-2} at 333 K. The concentration of MO solution was evaluated by measuring the change in maximum absorbance through TU-1810 UV-vis spectrophotometer.

3. Results and discussion

Fig. 1a shows XRD patterns of as-spun $Cu_{72-x}Y_{28}Ag_x$ ($x = 0$ and 2 at%) ribbons. Only a strong broad diffraction peak appeared around 39° in their patterns, indicating that the as-spun specimens have a fully amorphous structure. Fig. 1b displays the XRD patterns of as-dealloyed ribbons, the patterns exhibit crystalline diffraction peaks of (111), (200) and (220), which can be indexed to *fcc* Cu (JCPDS card no. 04-0836). It should be noticed that the peak positions of the sample synthesized by dealloying $Cu_{70}Y_{28}Ag_2$ amorphous ribbons have obvious left-shift comparing with those of the sample fabricated by dealloying $Cu_{72}Y_{28}$ ribbons. The phenomenon can be caused by the formation of *fcc* Cu-based solid solution in as-dealloyed $Cu_{70}Y_{28}Ag_2$ ribbons.

In view of the facts that Ag element can not be detected in XRD patterns of as-dealloyed $Cu_{70}Y_{28}Ag_2$ ribbons, the high resolution XPS spectrum of Ag 3d was measured to confirm the phase composition of the dealloying products. Fig. 1c presents Ag 3d spectra of the sample prepared by dealloying $Cu_{70}Y_{28}Ag_2$, the binding energies of Ag $3d_{3/2}$ and Ag $3d_{5/2}$ are observed at 374.5 and 368.5 eV, respectively. Obviously, the splitting energy of 6 eV is in agreement with the standard spectrum of Ag^m.[30] Combining this result with the XRD result, it can be concluded that as-dealloyed $Cu_{70}Y_{28}Ag_2$ ribbons are in form of *fcc* Cu–Ag solid solution.

Fig. 2a and b depicts SEM images of the samples by dealloying $Cu_{72}Y_{28}$ and $Cu_{70}Y_{28}Ag_2$ amorphous ribbons, respectively. The images all exhibit 3D bi-continuous and interpenetrating nanoporous structures. Based on the results of

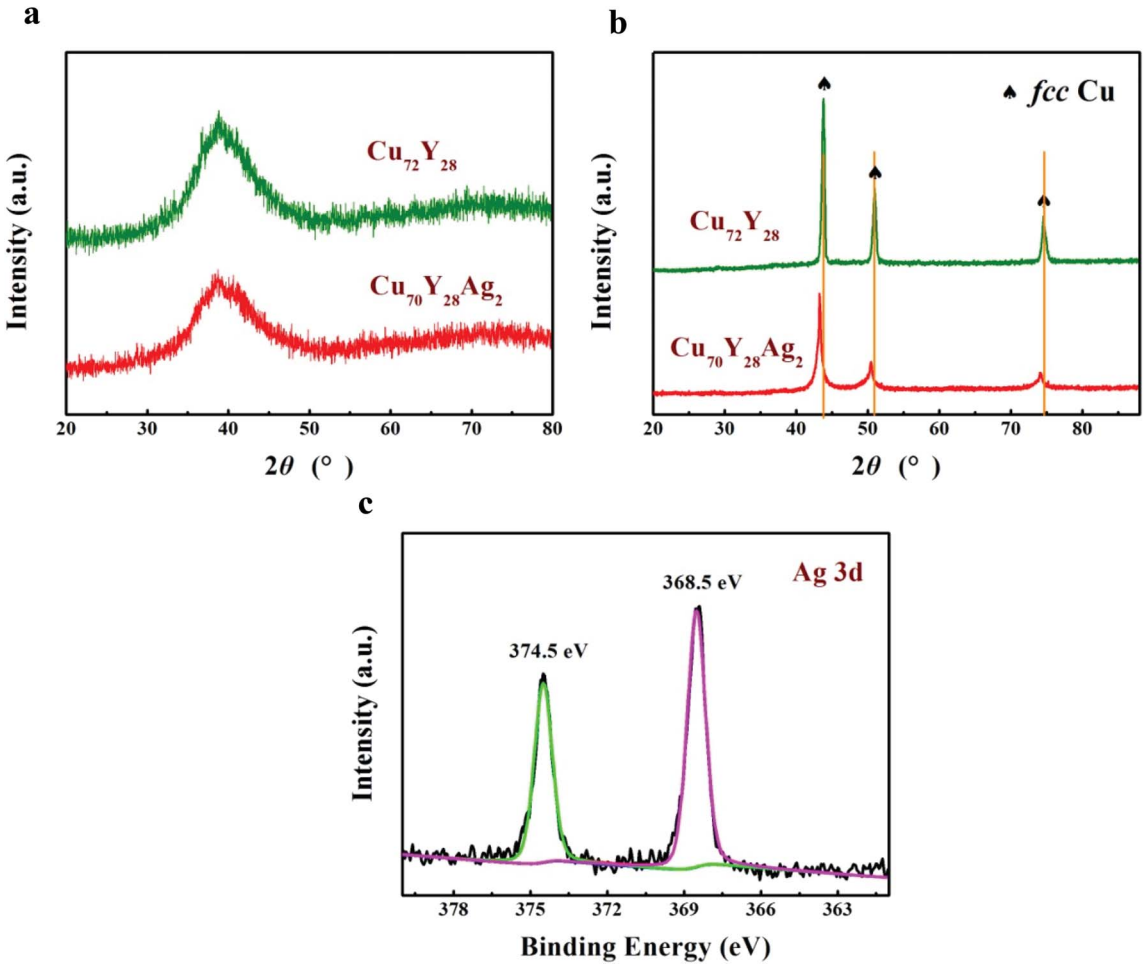

Fig. 1 XRD patterns of (a) Cu–Y(–Ag) metallic glasses and (b) the corresponding samples after dealloying in 1 M H_2SO_4 aqueous solution at 333 K for 90 min; (c) XPS Ag 3d spectra of as-dealloyed $Cu_{70}Y_{28}Ag_2$ ribbons.

SEM, XRD and XPS can confirm that nanoporous copper and nanoporous Cu–Ag solid solution have been successfully prepared. For convenience, the samples synthesized by dealloying $Cu_{72}Y_{28}$ and $Cu_{70}Y_{28}Ag_2$ are labeled as NPC and NPC and NPCS, respectively. It is obvious that the ligaments of NPCS is significantly finer than that of NPC, suggesting that the metal ligaments can be significantly refined by the substitution of 2 at% Ag element for Cu in Cu-based amorphous precursor. This is because that the surface diffusion coefficient of Ag atoms in a vacuum is two orders lower than that of Cu atoms.[11] Hence, Ag atoms which are uniformly distributed in amorphous precursor not only can recombine with Cu atoms to form the skeleton of the ligaments in the dealloying process, but also can act as a diffusion barrier to restrict the long distance diffusion of Cu atoms,[25] achieving the goals of refining the ligaments of nanoporous materials. Moreover, the EDS results show that the nanoporous material synthesized by dealloying Cu–Y metallic glasses is composed of Cu element, while the one fabricated by dealloying Cu–Y–Ag alloys consists of both Cu and Ag elements, indicating that Y has been completely removed from the precursor alloys and the remaining inert metal elements form a framework of nanoporous structure. The results agree well with the XRD and XPS results.

Fig. 2c and d presents the TEM images of NPC and NPCS. The images show that the samples consist of a bi-continuous pore-to-ligament nano-structure and NPCS has much finer ligament structure than NPC. The results are consistent with the SEM results. By measuring from TEM images, the sizes of ligaments of NPC and NPCS are estimated to be 370 and 45 nm, while the ones measured by previous SEM images are evaluated to be 402 and 65 nm, respectively (displayed in Table 1). The reason can be explained as follows: owing to the concentration gradient of H_2SO_4 solution in the corrosion ribbons, the dealloying samples have finer nanoporous structures in its internal region, which can be obtained by ion beam thinning and measured by TEM. Fig. 3 shows EDS element mapping of the NPCS sample, the images indicates that Cu and Ag elements are uniformly distributed in the as-dealloyed $Cu_{70}Y_{28}Ag_2$ ribbons and uniform Cu–Ag solid solution was formed. Table 1 shows that NPCS (S_{BET} = 8.34 $m^2\ g^{-1}$, V_p = 0.093 $cm^3\ g^{-1}$) with finer microstructure has far larger specific surface area and higher total pore volume than NPC (S_{BET} = 1.77 $m^2\ g^{-1}$, V_p = 0.050 $cm^3\ g^{-1}$), which are measured by BET method.

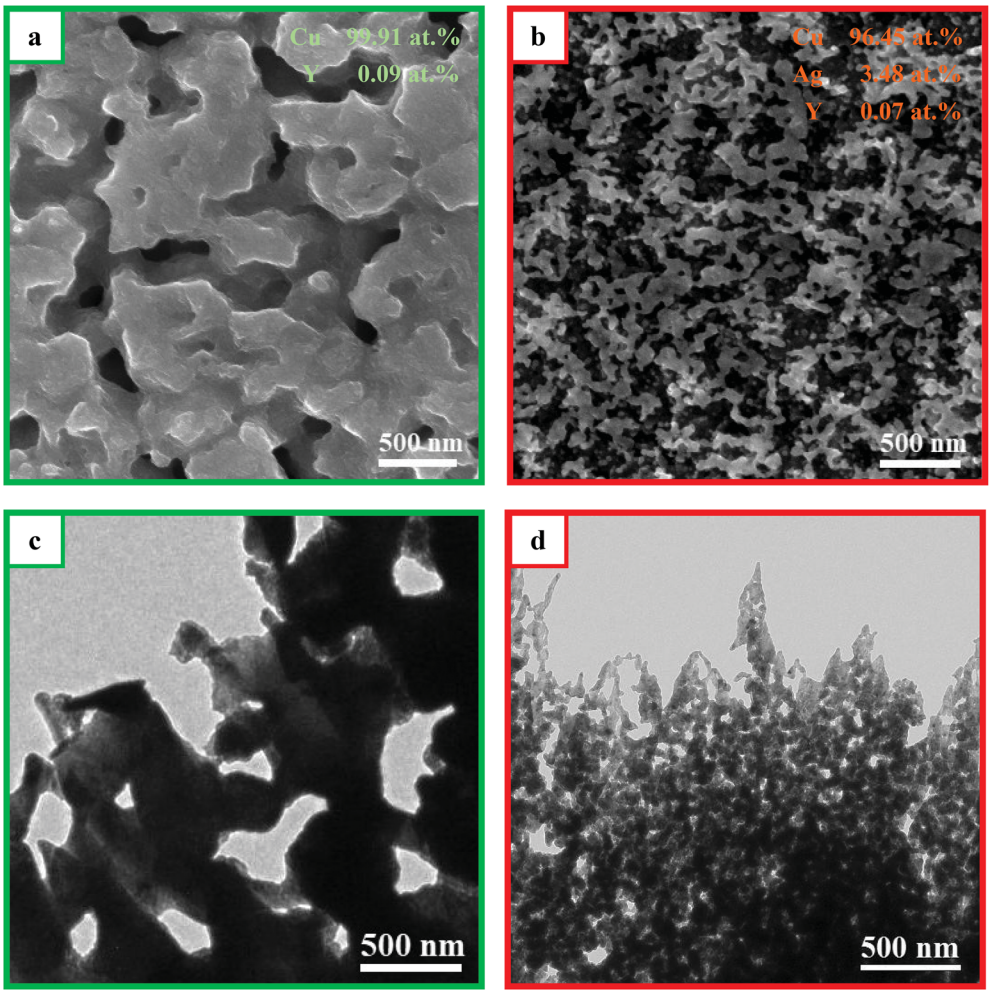

Fig. 2 SEM images of the samples prepared by dealloying (a) $Cu_{72}Y_{28}$ and (b) $Cu_{70}Y_{28}Ag_2$ metallic glasses in 1 M H_2SO_4 aqueous solution at 333 K for 90 min. TEM images of the samples: (c) NPC; (d) NPCS.

Table 1 The morphological features (ligament size measured by SEM (d_{SEM}), ligament size measured by TEM (d_{TEM}), specific surface area (S_{BET}) and total pore volume (V_p)) of the samples

Samples	d_{SEM} (nm)	d_{TEM} (nm)	S_{BET} ($m^2\ g^{-1}$)	V_p-total ($cm^3\ g^{-1}$)
NPC	402 ± 37.1	370 ± 35.0	1.77 ± 0.58	0.050
NPCS	65 ± 11.9	45 ± 10.6	8.34 ± 1.31	0.093

To investigate the catalytic activity of nanoporous Cu–Ag solid solution, the experiment of methyl orange (MO) sono-degradation was carried out. Fig. 4a shows the sonocatalytic degradation curves of MO. It can be seen that only 35.2% and 32.3% of MO were degraded over the commercial copper foil and silver foil within 15 min, respectively, while up to 63.6% and 81.0% of MO were decomposed over the NPC and NPCS sample within the same time, respectively. Obviously, nanoporous Cu-based material has higher catalytic activity compared to the pure metal foil. The reason can be attributed to 3D bi-continuous nanoporous structure of NPC and NPCS.

Fig. 4b demonstrates linear relationships between $\ln(C/C_0)$ and ultrasound irradiation time (t), revealing that these degradation processes obey pseudo-first-order kinetics. Therefore, Langmuir–Hinshelwood model (eqn (1))[31,32] can be used to calculate to the values of the reaction rate constant:

$$\ln(C/C_0) = -kt \quad (1)$$

where C is the concentration of MO at time t, C_0 is the initial concentration, k is the apparent reaction rate constant. The k values under different experiment conditions of no catalyst, NPCS without ultrasound, Ag foil, Cu foil, NPC and NPCS were evaluated to 0.004, 0.028, 0.034, 0.039, 0.086 and 0.131 min^{-1}. Evidently NPCS is the most effective, the reasons can be related to two points: (1) NPCS has much larger specific surface area compared with NPC and copper foil, which can provide more interfaces to facilitate interaction between the catalyst and dye molecules.[33] In addition, more cavitation bubbles can be formed on the surface of NPCS to produce ·OH because the surface of catalysts act as the nucleus for cavitation bubbles in the sono-catalytic process.[34] (2) NPCS has higher total pore

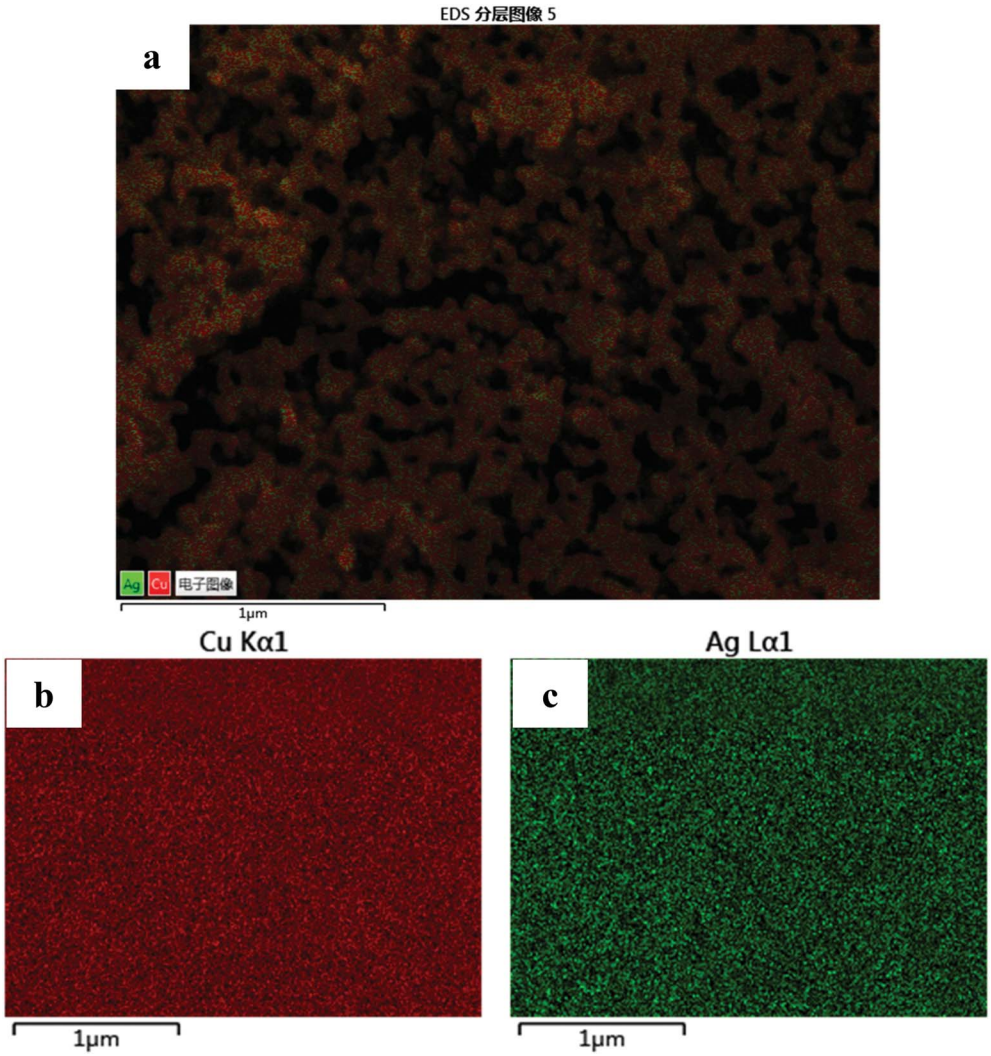

Fig. 3 (a) EDS element mapping of the NPCS sample; the distribution of each element: (b) Cu Kα, (c) Ag Lα.

volume than NPC and Cu foil, thus not only allowing the interior ligaments to maximize the absorption of acoustic energy and produce ·OH, but also providing more channels for diffusion and transportation of ·OH,[35] which play very important roles in the sono-catalytic degradation process. It should be noticed that the degradation rate of NPCS decreases extremely

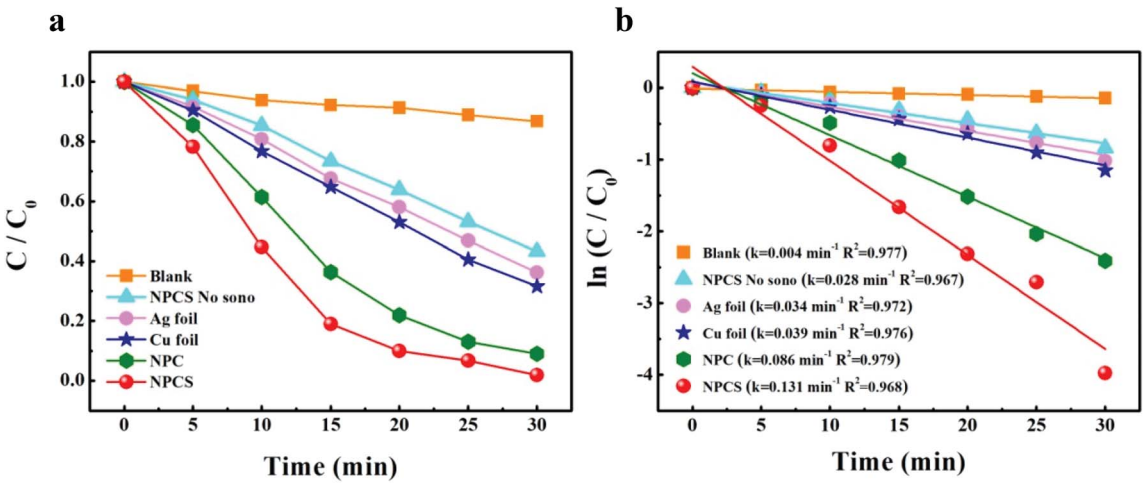

Fig. 4 (a) Sonocatalytic degradation of MO *versus* reaction time, (b) linear transform ln(C/C_0) of the kinetic curves of MO degradation.

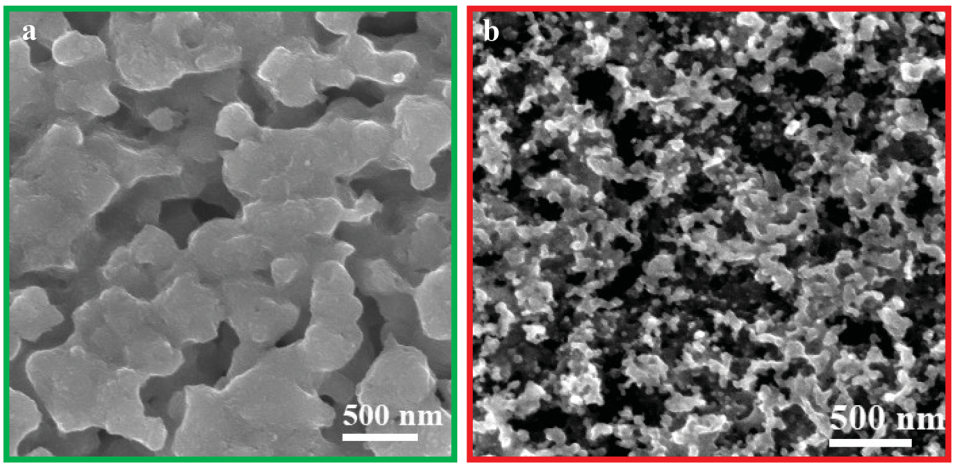

Fig. 5 SEM images of the nanoporous metal catalysts after catalytic reaction: (a) NPC; (b) NPCS.

when the ultrasound was removed, implying that the degradation of MO dye in this experiment is a sono-catalytic process.

Fig. 5 shows the SEM images of NPC and NPCS after reaction. It can be seen that only a few metal nanoparticles break away from the nanoporous metal and the structure of nanoporous metal partly break apart, indicating that the catalysts have certain stability in the structure.

The sono-Fenton-like process of NPCS is similar to that of NPC,[6,18] which can be described as follows: under the radiation of ultrasound, fine Cu–Ag ligaments react with H_2O_2 to generate Cu^+, Ag^+ and high activity hydroxyl radicals ($\cdot OH$), subsequently the Cu^+ which is produced in the previous step further react with H_2O_2 to form Cu^{2+} and $\cdot OH$. At the same time, Cu^{2+}, Cu^+ and Ag^+ combine with electrons (e^-) to be reduced back to Cu^+, Cu and Ag, respectively, thus allowing the sono-Fenton-like process to go and return in following a circle. Finally, $\cdot OH$ produced by this process decomposes MO molecules into oxidation product. The reactions can be described as eqn (2)–(7):

$$\text{Cu–Ag ligaments} + H_2O_2 + H^+ +))) \text{ (ultrasound)} = Cu^+/Ag^+ + H_2O + \cdot OH \quad (2)$$

$$Cu^+ + H_2O_2 + H^+ +))) \text{ (ultrasound)} = Cu^{2+} + H_2O + \cdot OH \quad (3)$$

$$Cu^{2+} + e^- = Cu^+ \quad (4)$$

$$Cu^+ + e^- = Cu \quad (5)$$

$$Ag^+ + e^- = Ag \quad (6)$$

$$\cdot OH + MO \rightarrow \text{oxidation product} \quad (7)$$

4. Conclusions

Nanoporous Cu–Ag solid solution (NPCS) with a 3D bi-continuous nanoporous structure was successfully prepared by dealloying $Cu_{70}Y_{28}Ag_2$ amorphous ribbons. The synthesized NPCS not only possesses much finer ligaments (d_{SEM} = 65 nm, d_{TEM} = 45 nm) than NPC fabricated by dealloying $Cu_{72}Y_{28}$ (d_{SEM} = 402 nm, d_{TEM} = 370 nm), but also presents higher sono-Fenton-like catalytic performance (k = 0.131 min^{-1}) compared to NPC (k = 0.086 min^{-1}) and Cu foil (k = 0.039 min^{-1}). The excellent sonocatalytic activity of NPCS can mainly be attributed to its larger specific surface area (8.34 $m^2\ g^{-1}$) and higher total pore volume (0.093 $cm^3\ g^{-1}$). Thus it can be seen that NPCS with both high sonocatalytic activity and good oxidation resistance has great potential in organic industry wastewater treatment.

Conflicts of interest

There are no conflicts to declare.

Acknowledgements

This work was supported by the Advanced Talents Funds of Nanjing Institute of Technology (Grant No. YKJ201809), the Science Foundation for the Excellent Youth Scholars of Jiangsu Province (BK20180106) and the Innovation Funds of Nanjing Institute of Technology (Grant No. CKJA201703).

References

1 S. P. Azerrad, M. Isaacs and C. G. Dosoretz, Integrated treatment of reverse osmosis brines coupling electrocoagulation with advanced oxidation processes, *Chem. Eng. J.*, 2019, **356**, 771–780.
2 L. Mansouri, C. Tizaoui, S. Geissen, *et al.*, A comparative study on ozone, hydrogen peroxide and UV based advanced oxidation processes for efficient removal of diethyl phthalate in water, *J. Hazard. Mater.*, 2019, **363**, 401–411.
3 J. Kang, S. Irmak and M. Wilkins, Conversion of lignin into renewable carboxylic acid compounds by advanced oxidation processes, *Renewable Energy*, 2019, **135**, 951–962.
4 A. Mossmann, G. L. Dotto, D. Hotza, *et al.*, Preparation of polyethylene-supported zero-valent iron buoyant catalyst

and its performance for Ponceau 4R decolorization by photo-Fenton process, *J. Environ. Chem. Eng.*, 2019, **7**, 102963.

5 X. Y. Zhang, J. F. Ma, C. H. Fan, *et al.*, Enhancement of photo-Fenton-like degradation of orange II by MnO_2/NiO nanocomposite with the synergistic effect from bisulfite, *J. Alloys Compd.*, 2019, **785**, 343–349.

6 N. Wang, Y. Pan, S. K. Wu, *et al.*, Fabrication of nanoporous copper with tunable ligaments and promising sonocatalytic performance by dealloying Cu-Y metallic glasses, *RSC Adv.*, 2017, **7**, 43255–43265.

7 Y. L. Min, K. Zhang, Y. C. Chen, *et al.*, Sonodegradation and photodegradation of methyl orange by $InVO_4/TiO_2$ nanojunction composites under ultrasonic and visible light irradiation, *Ultrason. Sonochem.*, 2012, **19**, 883–889.

8 A. Khataee, P. Gholami, B. Vahid, *et al.*, Heterogeneous sono-Fenton process using pyrite nanorods prepared by non-thermal plasma for degradation of an anthraquinone dye, *Ultrason. Sonochem.*, 2016, **32**, 357–370.

9 X. Y. Ma, Y. Q. Cheng, Y. J. Ge, *et al.*, Ultrasound-enhanced nanosized zero-valent copper activation of hydrogen peroxide for the degradation of norfloxacin, *Ultrason. Sonochem.*, 2018, **40**, 763–772.

10 P. Vaishnave, A. Kumar, R. Ameta, *et al.*, Photo oxidative degradation of azure-B by sono-photo-Fenton and photo-Fenton reagents, *Arabian J. Chem.*, 2014, **7**, 981–985.

11 E. Neyens and J. Baeyens, A review of classic Fenton's peroxidation as an advanced oxidation technique, *J. Hazard. Mater.*, 2003, **98**, 33–50.

12 B. Yao, D. Fleming, M. A. Morris, *et al.*, Structural control of mesoporous silica nanowire arrays in porous alumina membranes, *Chem. Mater.*, 2004, **16**, 4851–4855.

13 T. Kijima, T. Yoshimura, M. Uota, *et al.*, Noble-metal nanotubes (Pt, Pd, Ag) from lyotropic mixed-surfactant liquid-crystal templates, *Angew. Chem.*, 2003, **116**, 230–234.

14 M. J. Pryor and J. C. Fister, The mechanism of dealloying of copper solid solutions and intermetallic phases, *J. Electrochem. Soc.*, 1984, **131**, 1230–1235.

15 J. Erlebacher, An atomistic description of dealloying porosity evolution, the critical potential, and rate-limiting behavior, *J. Electrochem. Soc.*, 2004, **151**, C614–C626.

16 P. Rizzi, F. Scaglione and L. Battezzati, Nanoporous gold by dealloying of an amorphous precursor, *J. Alloys Compd.*, 2014, **586**, S117–S120.

17 Y. Jin, R. Li and T. Zhang, Formation of nanoporous silver by dealloying Ca-Ag metallic glasses in water, *Intermetallics*, 2015, **67**, 166–170.

18 N. Wang, Y. Pan and S. K. Wu, Relationship between dealloying conditions and coarsening behaviors of nanoporous copper fabricated by dealloying Cu-Ce metallic glasses, *J. Mater. Sci. Technol.*, 2018, **34**, 1162–1171.

19 J. Erlebacher, M. J. Aziz, A. Karma, *et al.*, Evolution of nanoporosity in dealloying, *Nature*, 2001, **410**, 450–453.

20 Z. H. Zhang, Y. Wang, Z. Qi, *et al.*, Generalized fabrication of nanoporous metals (Au, Pd, Pt, Ag, and Cu) through chemical dealloying, *J. Phys. Chem. C*, 2009, **113**, 12629–12636.

21 M. Hakamada, H. Nakano, T. Furukawa, *et al.*, Hydrogen storage properties of nanoporous palladium fabricated by dealloying, *J. Phys. Chem. C*, 2010, **114**, 868–873.

22 D. V. Pugh, A. Dursun and S. G. Corcoran, Formation of nanoporous platinum by selective dissolution of Cu from $Cu_{0.75}Pt_{0.25}$, *J. Mater. Res.*, 2003, **18**, 216–221.

23 R. Yamaguchi, S. Kurosu, M. Suzuki, *et al.*, Hydroxyl radical generation by zero-valent iron/Cu (ZVI/Cu) bimetallic catalyst in wastewater treatment: Heterogeneous Fenton/Fenton-like reactions by Fenton reagents formed in situ under oxic conditions, *Chem. Eng. J.*, 2018, **334**, 1537–1549.

24 L. Hurtado, R. Romero, A. Mendoza, *et al.*, Paracetamol mineralization by photo Fenton process catalyzed by a Cu/Fe-PILC under circumneutral PH conditions, *J. Photochem. Photobiol., A*, 2019, **373**, 162–170.

25 Z. H. Dan, F. X. Qin, A. Makino, *et al.*, Fabrication of nanoporous copper by dealloying of amorphous Ti-Cu-Ag alloys, *J. Alloys Compd.*, 2014, **586**, S134–S138.

26 E. S. Park, H. J. Chang, D. H. Kim, *et al.*, Effect of the substitution of Ag and Ni for Cu on the glass forming ability and plasticity of $Cu_{60}Zr_{30}Ti_{10}$ alloy, *Scr. Mater.*, 2006, **54**, 1569–1573.

27 Z. H. Dan, F. X. Qin, Y. Sugawara, *et al.*, Fabrication of nanoporous copper by dealloying amorphous binary Ti-Cu alloys in hydrofluoric acid solutions, *Intermetallics*, 2012, **48**, 14–20.

28 J. S. Yu, Y. Ding, C. X. Xu, *et al.*, Nanoporous metals by dealloying multicomponent metallic glasses, *Chem. Mater.*, 2008, **20**, 4548–4550.

29 R. Li, N. Wu, J. J. Liu, *et al.*, Formation and evolution of nanoporous bimetallic Ag-Cu alloy by electrochemically dealloying Mg-(Ag-Cu)-Y. metallic glasses, *Corros. Sci.*, 2017, **119**, 23–32.

30 C. D. Wagner, W. M. Riggs, and L. E. Davis, *et al.*, *Handbook of X-ray photoelectron spectroscopy*, Perkin-Elmer, Eden Prairie, 1979.

31 V. Scuderi, G. Amiard, S. Boninelli, *et al.*, Photocatalytic activity of CuO and Cu_2O nanowires, *Mater. Sci. Semicond. Process.*, 2016, **42**, 89–93.

32 N. Wang, Y. Pan, T. Lu, *et al.*, A new ribbon-ignition method for fabricating p-CuO/n-CeO_2 heterojunction with enhanced photocatalytic activity, *Appl. Surf. Sci.*, 2017, **403**, 699–706.

33 S. Kumar and A. K. Ojha, Oxygen vacancy induced photoluminescence properties and enhanced photocatalytic activity of ferromagnetic ZrO_2 nanostructures on methylene blue dye under ultra-violet radiation, *J. Alloys Compd.*, 2015, **644**, 654–662.

34 H. Zhao, G. M. Zhang and Q. L. Zhang, MnO_2/CeO_2 for catalytic ultrasonic degradation of methyl orange, *Ultrason. Sonochem.*, 2014, **21**, 991–996.

35 Z. Deng, C. Zhang and L. Liu, Chemically dealloyed MgCuGd metallic glass with enhanced catalytic activity in degradation of phenol, *Intermetallics*, 2014, **52**, 9–14.